Desalination and Water Treatment
www.deswater.com

doi: 10.1080/19443994.2015.1079250

57 (2016) 16161–16176
July

Taylor & Francis
Taylor & Francis Group

Interface behavior of PbO_2 on pure lead and stainless steel as anode for dye degradation

Ines Elaissaoui, Hanene Akrout*, Latifa Bousselmi

Laboratory of Wastewater Treatment, Center of Water Research & Technology (CERTE), Borj Cédria PB 273, Soliman 8020, Tunisia, Tel. +216 79 325 044; email: issaouines@yahoo.fr (I. Elaissaoui), Tel. +216 79 325 044; Fax: +216 79 325 802; email: hanene.akrout@yahoo.com (H. Akrout), Tel. +216 79 325 044; email: latifa.bousselmi@certe.rnrt.tn (L. Bousselmi)

Received 9 September 2014; Accepted 15 July 2015

ABSTRACT

PbO_2 films are electrodeposited by the galvanostatic (G) and pulsed current (P) methods on lead and stainless steel (AS30), respectively. They are used as electrodes for electrochemical degradation of Amaranth dye. The scanning electron microscope, atomic force microscope, and X-ray diffraction analyses revealed the dominance of β-PbO_2 form in two anodes and the absence of the form tet-PbO and $PbSO_4$ in AS30 substrate that have more amorphous shape and less roughness (200 nm). A poor lead oxide adhesion on AS30 substrate is detected. Cyclic voltammetry results showed that the absence of oxidation peak in the case of AS30/PbO_2 anode is related to the oxidation of $PbSO_4$ to β-PbO_2. EIS results demonstrated that the pH influences largely PbO_2 layer. Concerning E123 degradation, 95 and 91% of color removal (82 and 76% of Chemical oxygen demand removals) were achieved using Pb/PbO_2 and AS30/PbO_2 anodes, respectively. In this case, current efficiency has kept relatively a high value assuming less energy consumption.

Keywords: PbO_2; Stainless steel; EIS interface; Degradation

1. Introduction

The textile dyeing and finishing processes, that need large quantities of water, are considered as one of the most polluting textile industrial activities [1]. Related wastewater includes dyes as azo dyes which are characterized by a stable chemical structure. Azo groups structures could not be eliminated by conventional methods [1,2].

In this context, various advanced oxidations processes such as photocatalytic degradation [3], electrocoagulation [4], and ozonation [5] are used for treating textile wastewater. Anodic oxidation (AO) is attracting more and more attention as efficient methods to remove toxic organic compounds from wastewater [6] and textile effluents [7]. AO is based on the electrogeneration of hydroxyl radicals as environmentally friendly oxidants. The removal of electrochemical processes is strictly related to the operating conditions, more precisely to the electrode materials [8,9].

Thus, proper selection of electrodes is the key factor in the effectiveness of this technology. In the case of dyestuffs, different anodes have been investigated, such as platinum [10], glassy carbon [11], and boron doped diamond [4,12–14]. Applying lead dioxide (PbO_2) as an active surface was tested on same substrates like titanium [15,16], stainless steel [17], and

---

*Corresponding author.

carbon [18]. As a matter of fact, several scientists have focused more on PbO_2 due to its high electronic conductivity, chemical stability in corrosive media [19], and relatively high over potential for the oxygen evolution reaction [6,20]. Many reports involving dye wastewaters treatment have been investigated; among them we can find the use of AO using PbO_2 anodes. Zhou et al. [21] which studied the influence of electrochemical methods on PbO_2 and they have confirmed that the lead dioxide, formed by the galvanostatic method, has more impact and a continuous structure which exhibited a low charge transfer resistance. Other scientists focused on the influence of pH media deposition/dissolution of PbO_2 on BDD support. They found that strong alkaline electrolyte can conduct to the dissolution of PbO_2. However, in an acidic and neutral media, PbO_2 morphology has a good correlation with the obtainment of high oxygen over potential [22]. Mukimin et al. [23] used PbO_2 anode for electrodegradation of Remozol Brilliant Blue R (RB.19), which is very effective in destructing even persistent dyes. They confirmed that pH, and NaCl concentration is the key variables that affect the degradation performance of RB.19 by electrolysis. Abaci et al. [24] prepared different structures of PbO_2 surfaces and described the electrochemical degradation of phenol. The experimental results showed that β structure of PbO_2 has higher performance than that of the α structure on phenol degradation. Also, the higher crystallinity of pure β-PbO_2 has increased the efficiency of the phenol degradation process.

A frequently used method is to dope the PbO_2 layer. For exemple, Hao et al. [25] prepared PbO_2 electrodes doped by Fe, Ni, and Ag. The Fe-doped PbO_2 has the longest accelerated life test due to its dense surface, and the Ni-doped PbO_2 has the highest oxygen evolution and has demonstrated the best performance for the phenol degradation. Andrade et al. compared the performance of PbO_2 doped by Fe and F (together or separately) in electro-oxidation of the blue Reactive 19 dye. The results showed F-doped PbO_2 electrodes that are chemically and electrochemically stable, are suitable to be used in the electrochemical treatment of dye wastewater [26].

For a further enhancement of the electrocatalytic proprieties of PbO_2 during various anodic reactions, the incorporation of metal oxide, such as TiO_2 [27], RuO_2 [28], CeO_2 [18], SnO_2 [11,29,30], and ZrO_2 [31], into lead dioxide matrix was realized. These researches have indicated that the performance of PbO_2 electrode is influenced significantly by metal oxide particles. Nevertheless, some restrictions are imposed on the use of pure lead as a substrate according to the possibility of Pb release during the decontamination process [32]. The substitution of Pb by other environment friendly substrates is very interesting for potential application. The stainless steel is the most common material used in the industrial sector for its low cost and good corrosive stability, and non-toxicity compared to other materials [33].

The aim of this work is to use stainless steel (AS30) as substrate for electrodeposited PbO_2 layer, it is compared to Pb/PbO_2 electrode considered as a reference to study the morphology obtained, the electrochemical interface behavior, and the degradation power of AS30/PbO_2 anode.

Oxide layers deposited on both substrates AS30 and lead are characterized by DRX, scanning electron microscope (SEM), and atomic force microscope (AFM). The electrochemical behavior of the two electrodes performed is studied by cyclic voltammetry (CV). Besides, Electrochemical Impedance Spectroscopy (EIS) is used to compare film resistance and transfer charge resistance measured at the substrate, and the oxide lead layer interface. Furthermore, electro-oxidation proprieties are also tested for the degradation of synthetic wastewater containing Amaranth dye as a pollutant model.

2. Experimental

2.1. Substrates

A pure lead ($Pb > 99.9\%$) and stainless steel (AS30) are used as two substrates for the electrodepostion of lead dioxide. Surfaces are carefully polished with abrasive papers, rinsed with doubly distilled water and degreased with acetone.

2.2. Chemicals

Chemicals, including $Pb(NO_3)_2$ (Panerac Quimica SA-99%), HNO_3 (Sigma-Aldrich-95–97%), and sulfuric acid (Sigma-Aldrich-95–97%), are used for electrochemical treatment or deposition, and for initial adjustment of pH (equal to 2) of samples solution. Sodium sulfate (Na_2SO_4, Sigma-Aldrich 99%) is used for supporting electrolyte (0.1 M) during the degradation. The dye pollutant is Amaranth (E123.) (Sigma-Aldrich) azo dye having a molecular formula $C_{20}H_{11}N_2Na_3O_{10}S_3$ and a molar mass of 606.48 g mol^{-1} (Fig. 1(a)). The concentration of dye is fixed at 0.05 mM in 0.1-M Na_2SO_4. The coloration is attributed to azo groups accountable to the red-brown dye (E123) with bond absorption in the visible region ($\lambda = 520$ nm) (Fig. 1(b)). It is ascribed to the absorption of the $n \rightarrow \pi^*$ transition related to

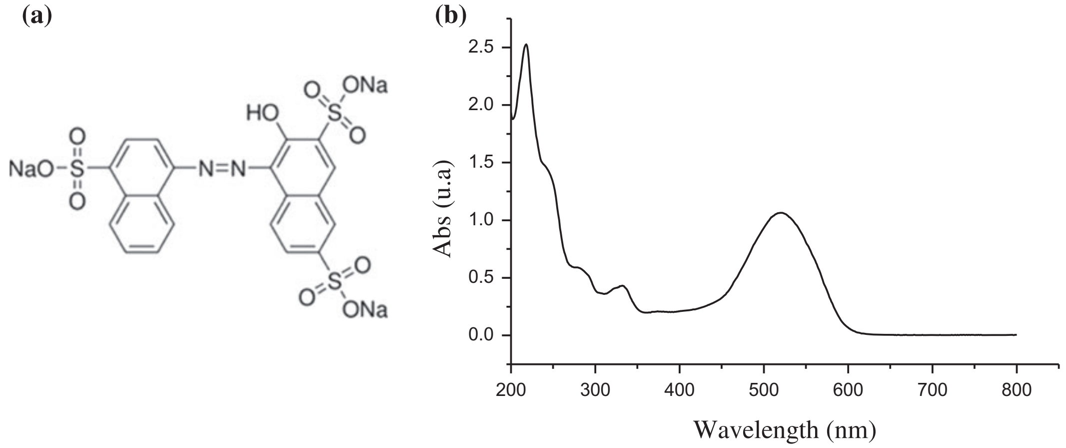

Fig. 1. (a) Structural formula and (b) UV spectrum of Amaranth (CEE No. E123).

–N=N– group. Distilled water, acetone (Richel), and doubly distilled water are used for cleaning the electrode before experiments.

2.3. *Electrodeposition of lead dioxide*

2.3.1. *Preparation of Pb/PbO$_2$ electrode*

Experiments were carried out on pure lead foil of 2.25 cm^2 surface. A classical three-electrode glass cell is used, and lead substrate electrode is immersed in sulfuric acid solution with platinum as a counter electrode and a saturated calomel electrode as a reference. Immediately before each experiment, the exposed-lead surface is cleaned. The PbO$_2$ layer is prepared at the current density of 10 mA cm^{-2} for 1.5 h in a 10% H$_2$SO$_4$ solution at 25℃ [11,21,30].

2.3.2. *Preparation of AS30/PbO$_2$ electrode*

PbO$_2$ was directly synthesized by the pulsed current method on the AS30 surface with 2.25 cm^2 area using a 0.5 M HNO$_3$ and a 0.5 M Pb(NO$_3$)$_2$ solutions. For each electrode, 170 pulses were applied as shown in Fig. 2 [34] (pulse height of 30 mA cm^{-2}, pulse width of 1 s at 30 mA cm^{-2} and relaxation time of 5 s at zero current).

2.4. *Morphology SEM, AFM, and XRD*

The morphology analysis of the PbO$_2$ layer was observed by a JSM-6490LV SEM at an accelerating voltage of 5 KV. X-ray diffraction (XRD) patterns of the PbO$_2$ layer are characterized by X-ray diffractometer using Cu Kα anode ($\lambda_1 = 1.5405980$). AFM-STM Digital III-D3100 mode tapping is used to determinate the roughness parameters of the samples and to analyze the electrodes shape.

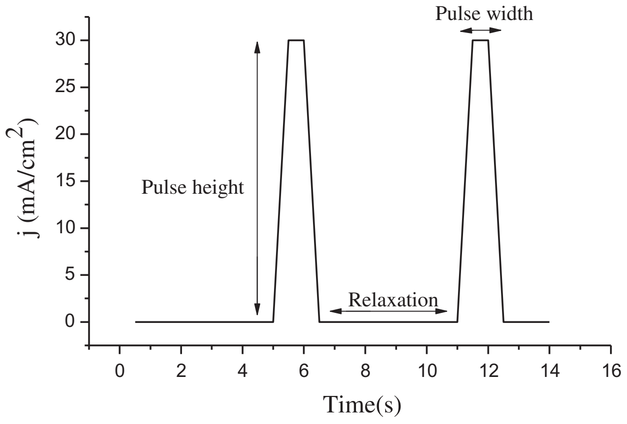

Fig. 2. Two-first pulsed current diagram of stainless steel in 0.5 M HNO$_3$ and 0.5 M Pb(NO$_3$)$_2$.

2.5. *Cyclic voltammetric and EIS measurements of Pb/PbO$_2$ and AS30/PbO$_2$ electrodes*

All electrochemical experiments are carried out in a conventional three-electrode cell. CV tests are conducted using voltammetric analyzer (Voltalab PGZ 301), in the potential region from 0.7 to 2.0 V at a scan rate of 50 mV s^{-1} in 0.5 M sulfuric acid. Electrochemical impedance spectroscopic data were carried out and fitted with a Z-simpwin 3.2 electrochemical workstation in the frequency ranging from 100 kHz to 3 Hz under a sinusoidal wave excitation of 5 mV amplitude. Impedance spectra are recorded at the open circuit potential after 15 min of immersion of electrode in two different electrolytes: H_2SO_4 (0.5 M) and Na_2SO_4 (0.1 M). The surface area of each electrode is equal to 2.25 cm^2. In order to achieve the reproducibility of EIS measurements, two samples were prepared and used in each interface studied and obtained in the range of frequency (100 kHz–3.16 Hz).

2.6. Anodic oxidation

Electrochemical degradation is conducted in one compartment plexiglass cell that contains Pb/PbO_2 or $AS30/PbO_2$ electrode as an anode and stainless steel (AS30) as a cathode. Both of the electrodes are disks with 12.56 cm^2 of surface; this high surface is used for more efficiency in the degradation of the dye, the interelectrode gap is fixed at 2 cm. The AO of Amaranth dye is realized galvanostatically by a power supply (PS500 Adamant Technologies) with applying current density of 25 mA cm^{-2}, and a peristaltic pump (Heidolph) allowing a flow rate of 138 l h^{-1}, and the recirculation of the dye solution. Experiments are carried out at 420 min electrolysis time in two initially pH: acidic (pH 2) and natural pH in Na_2SO_4 solution as an electrolyte support.

During the experiments, samples are drawn from the bulk of the reservoir at different times to be analyzed (All samples are filtered before different analysis). The discoloration of Amaranth is followed by UV–visible spectrophotometry analysis (Thermospectronic UV1), and the mineralization by measurement of Chemical oxygen demand (COD) is determined using the reactor digestion method based on the method of acidic oxidation by bichromate [9]. The decay of the COD is calculated from the following equation [35]:

$$\text{COD decay } (\%) = \frac{\Delta\text{COD}}{\text{COD}_0} \times 100 \quad (1)$$

where ΔCOD is the corresponding removal in COD (mg O_2 L^{-1}), and COD_0 is the initial value before treatment.

Experimentally, the discoloration efficiency or percentage of color removal during the treatment of dyes wastewater is determined by the expression [36]:

$$\text{Color removal } (\%) = \frac{\text{ABS}_0 - \text{ABS}_t}{\text{ABS}_0} \times 100 \quad (2)$$

where ABS_0 and ABS_t, respectively, are the average absorbance before and after an electrolysis time t at the maximum visible wavelength ($\lambda_{max} = 520$ nm) of the model dye.

Additionally, the limiting current can be estimated from the value of COD for AO of a real wastewater, as indicated by Panizza and Cerisola [7,13].

$$I_{\text{lim}}(t) = 4FAk_{\text{m}}\text{COD}_t \quad (3)$$

where $I_{lim}(t)$ is the limiting current (A) at a given time t, 4 is the number of the exchanged electrons, A is the electrode area (m^2), F is the Faraday constant, k_m is the average mass transport coefficient in the electrochemical reactor (m s^{-1}), (according to the literature for PbO_2, $k_m = 2.0 \times 10^{-5}$ m s^{-1} [20]), and COD_t is the chemical oxygen demand (mol O_2 m^{-3}) at a given time t. I_{lim} is equal to 0.907 mA cm^{-2} for the two substrates (Lead and stainless steel).

The current efficiency (C.E, in %) at a given time t for the electrochemical oxidation is determined using the expression [37]:

$$\text{C.E} = \frac{(\text{COD}_0 - \text{COD}_t)}{8It} \times F \times V_s \times 100 \quad (4)$$

I is the average applied current (in A), and V_s is the solution volume (in L).

The specific energy consumption (E_c, in KWh g COD^{-1}) is obtained as follows [38]:

$$E_c = \frac{I \times V \times t}{(\Delta\text{COD}) \times V_s} \quad (5)$$

where V is the average cell voltage (in V), t is the electrolysis time (h), and ΔCOD is the decay in COD (in g O_2 L^{-1}).

3. Results and discussions

3.1. Morphology and structure of PbO_2 film

3.1.1. SEM and AFM

The microstructure of PbO_2 anodic layer, electrodeposited on lead and stainless steel are tested by SEM technique. Fig. 3 represents micrograph samples of the PbO_2 layer electrodeposited on Pb under two different views: 200 and 20 μm, respectively, in the indexed Fig. 3(a) and (b). All particles have shown an agglomeration with limited individual particle boundary. The electrodeposited PbO_2 microparticles, on lead, present two crystalline structures β-PbO_2 and α-PbO_2, where β-PbO_2 is the tetragonal structure and α-PbO_2 is the orthorhombic structure.

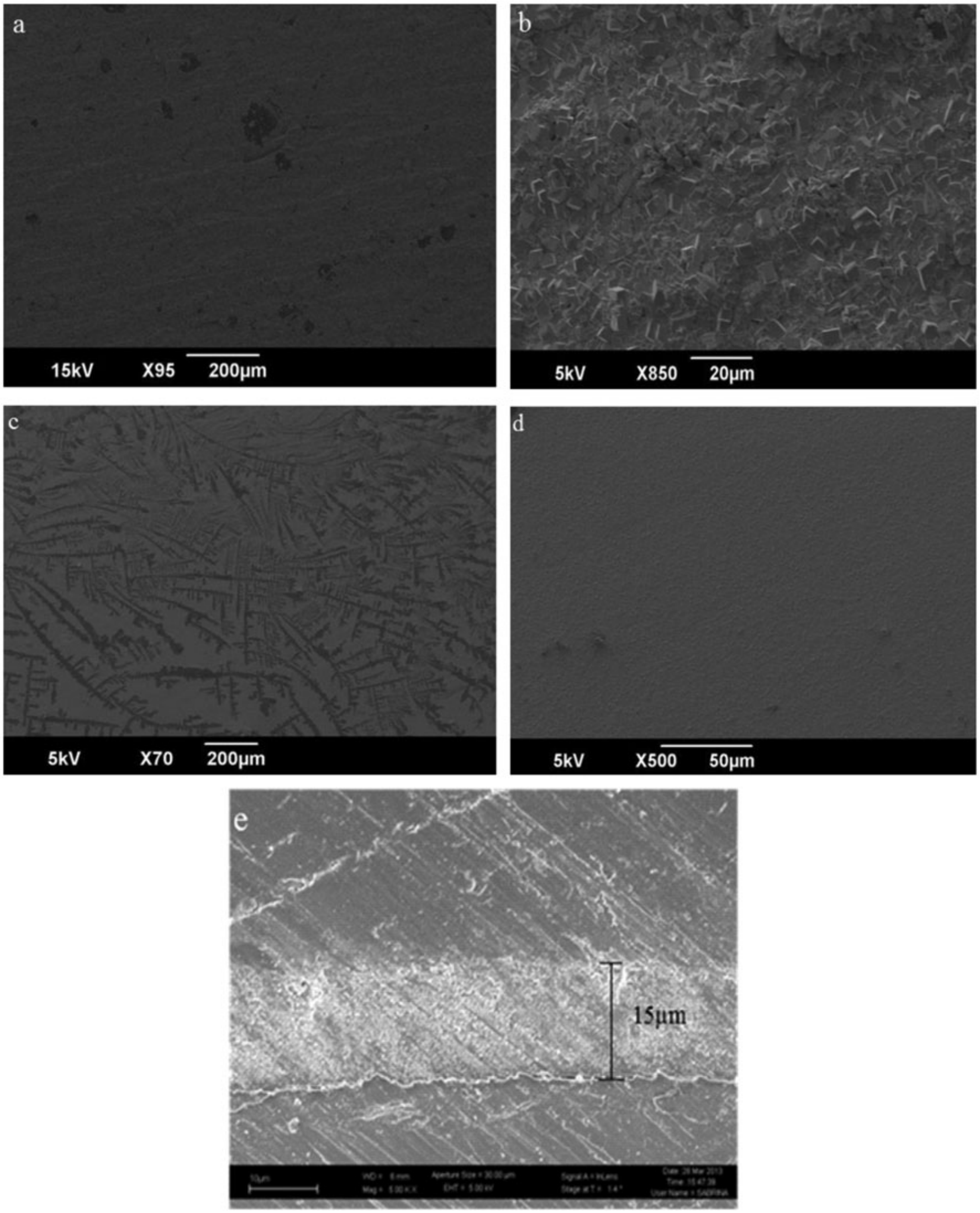

Fig. 3. SEM image of the thin film of PbO_2 on Pb anode: [(a) 200 μm and (b) 20 μm sizes] and on stainless steel: [(c) 200 μm, (d) 50 μm, and (e) sectional view].

In β-PbO_2 structures, neighboring octahedral shares opposite edges which results the formation of octahedral linear chains. However, in the α-PbO_2 structures, neighboring octahedral shares no opposite surfaces, in such case Zig-Zag chains are formed [21,39]. According to the AFM analysis (Fig. 4), the β-PbO_2 structures are more dominant one in PbO_2 electrodeposited layer on lead.

Fig. 4(a) shows the three-dimensional AFM images of PbO_2 layer on Pb anode, average particles size is

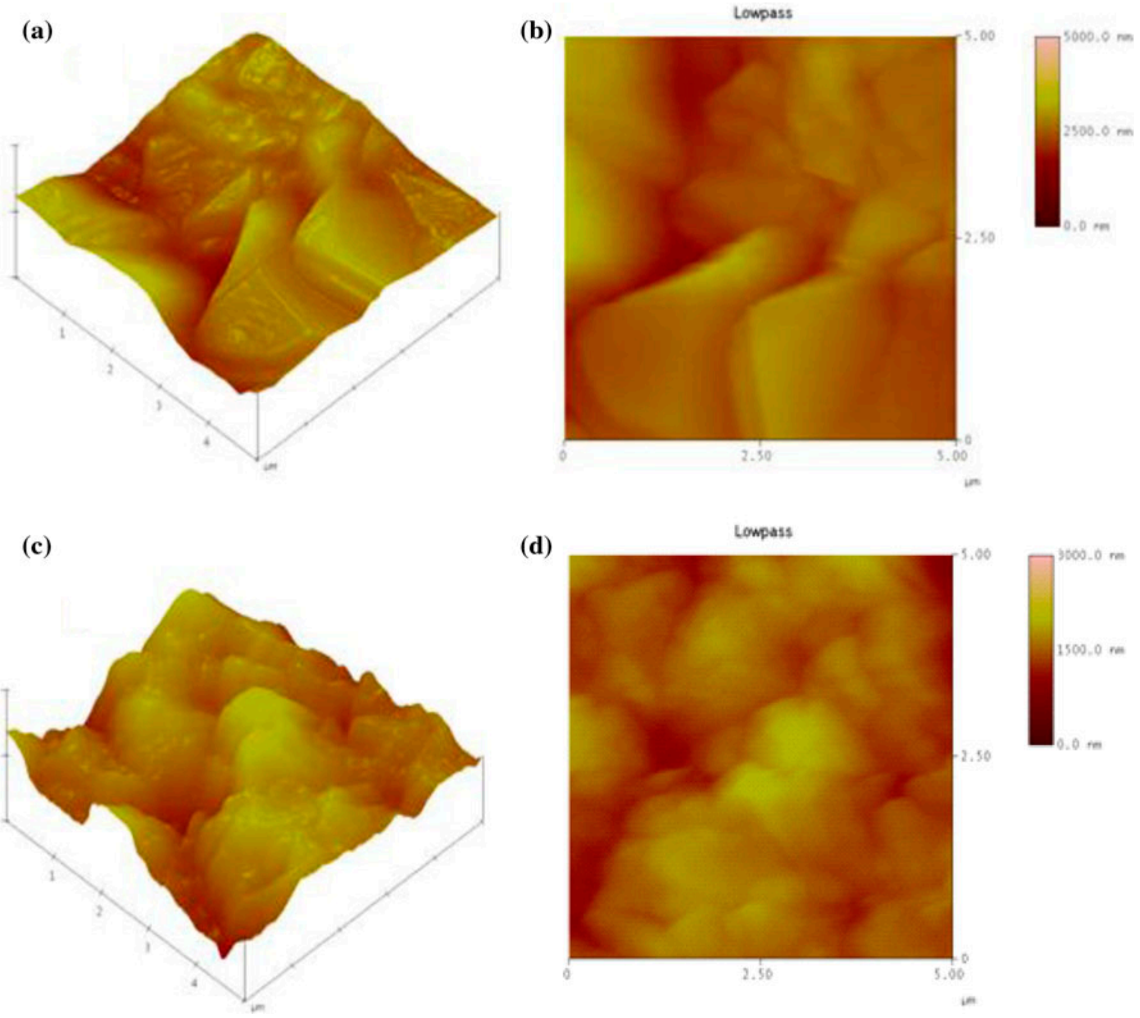

Fig. 4. Three-dimensional AFM images (a) and roughness (b) of PbO_2 layer electrodeposited on lead. Three-dimensional AFM images (c) and roughness (d) of PbO_2 layer electrodeposited on stainless steel.

about 2.5 µm and the film thickness is about 5 µm. The roughness of the dioxide lead film (Fig. 4(b)) is in the range of 297 nm, and most microparticles are within the range of 2–3 µm as shown in Fig. 4(b). A small imperfection is detected in the film which resides in low covered PbO_2 surfaces (Fig. 4(a)).

In the case of stainless steel substrate, the film has a good uniformity and a better coverage compared to lead substrate (SEM of Fig. 3(d)). A SEM sectional observation is realized as there are different substrates and oxide layer materials. In fact, limited adhesion is observed between the film and the stainless steel (Fig. 3(e)). This can be attributed to the passive layer formed instantly before electropulsed layer. The AFM image of PbO_2 thin films presents a different shape than that of the Pb/PbO_2, more amorphous layer is obtained and it could be observed in Fig. 4(d) with a roughness in the range of 200 nm.

3.1.2. X-ray diffraction

Fig. 5(a) shows the XRD diagram relative to PbO_2 electro-deposited anodic layer on Pb in H_2SO_4 solution. The obtained peaks are blended to crystalline forms: $PbSO_4$, 2θ equal to 20.6, 29.5, and 44.45 [21,40], Tet-PbO 2θ equal to 26.5 [13], α-PbO_2 at 2θ equal to 23, 27.5, 33, and 43.56 [13,21]. The crystalline structure is also confirmed to be bulk β-PbO_2 at 2θ equal to 25.4, 31.1, 32.2, 52, 62, and 65 [13,40]. Accordingly, in H_2SO_4 solution, the overall PbO_2 formation reaction involves three steps [21]:

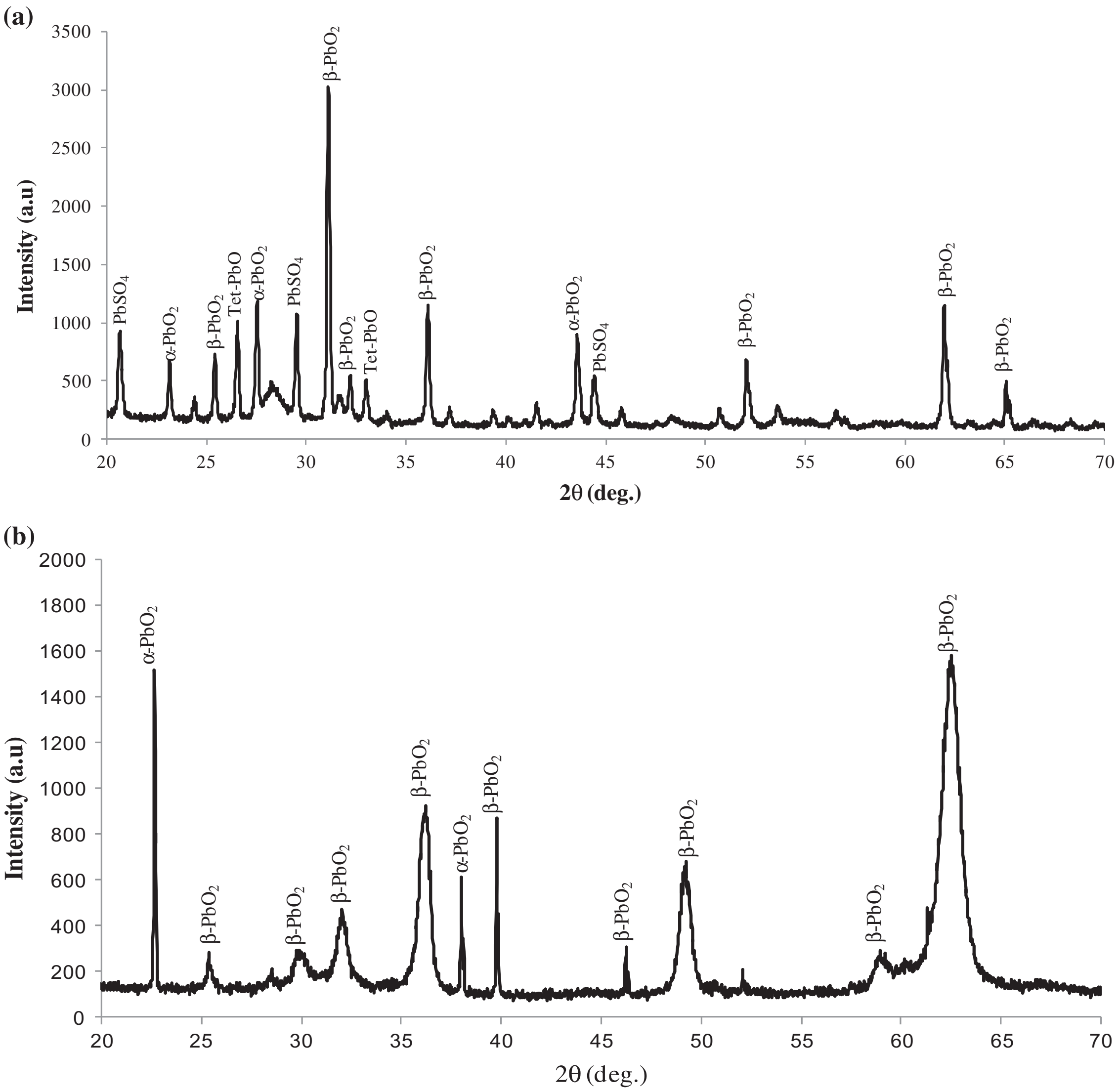

Fig. 5. XRD spectra of Pb/PbO$_2$ anode (a) and AS30/PbO$_2$ anode (b).

First Pb is oxidized to PbO and PbO·PbSO$_4$ (Eqs. (6) and (7)).

$$Pb + H_2O \rightarrow \text{tet-PbO} + 2e^- + 2H^+ \quad (6)$$

$$2Pb + SO_4^{2-} + H_2O \rightarrow PbO \cdot PbSO_4 + 2H^+ + 4e^- \quad (7)$$

The second step is the formation of α-PbO$_2$ and β-PbO$_2$ that are the results of the oxidation of PbO and PbSO$_4$, respectively.

$$PbO + H_2O \rightarrow \alpha\text{-}PbO_2 + 2H^+ + 2e^- \quad (8)$$

$$PbSO_4 + 2H_2O \rightarrow \beta\text{-}PbO_2 + SO_4^{2-} + 4H^+ + 2e^- \quad (9)$$

The third step consists in the oxidation of α-PbO$_2$ to β-PbO$_2$ [7,20,34].

$$\alpha\text{-}PbO_2 \rightarrow \beta\text{-}PbO_2 \quad (10)$$

Based on the PbO$_2$ electropulsed on stainless steel XRD pattern as shown in Fig. 5(b), there is a mixture of β-PbO$_2$ and α-PbO$_2$. In addition, it is obvious that β-PbO$_2$ is predominant and forms at 2θ equal to 25.4, 29.7, 32, 36.2, 39.7, 46.2, 49.3, 58.7, and 62.5 [18,34], while α-PbO$_2$ is found at 2θ equal to 22.6 and 38 [18]. It is generally believed that acidic media are favorable for β-PbO$_2$, whereas α-PbO$_2$ is preferably deposited from an alkaline solution [41]. We have noticed also the absence of tet-PbO and $PbSO_4$ forms. The inner tet-PbO layer is formed due to the impermeability of $PbSO_4$ layer in the presence of SO_4^{2-} ions. Only Pb^{2+}, OH^-, and H^+ ions can move across this film [41]. This is attributed to the presence of the tet-PbO forms that could improve their microstructure, diminish their inner stress, and enhance their adhesion.

The peaks of β-PbO_2 structure on lead have higher intensities than the β-PbO_2 structure on stainless steel substrate. In addition, the diffractive peaks become wider in the case of Pb/PbO_2 anode.

3.2. Electrochemical behavior of Pb/PbO_2 and $AS30/PbO_2$ anodes

3.2.1. Cyclic voltammetry

The mechanism of anodic Pb electrode oxidation in H_2SO_4 solution is very complicated since the reaction includes many chemical and electrochemical steps, species, and intermediates such as PbO_x, OH^-, and O^{2-}. Oxygen evolution involves high intermediate energy and complicated reaction pathways [42].

Typically, voltammetric curves of pure lead in sulfuric acid (0.5 M), limited by hydrogen and oxygen evolution processes, exhibit two peaks at the first cycle; as shown in Fig. 6(a) which is related to the oxidation of $PbSO_4$ to PbO_2 (usually β-form) at a potential of 1.83 V/ECS and the oxygen evolution. Then, one cathodic peak appears at the second cycle which is related to the reduction of PbO_2 to $PbSO_4$ at 1.25 V/ECS [43]. Thus, metallic lead surface is exposed, and can be oxidized by sulfuric acid.

Fig. 6(b) shows the typical cyclic voltammogram of the PbO_2 anodic layer electrodeposited on lead. The curve depicts two anodic peaks at the potentials 1.5 V/ESC and 1.85 V/ESC, respectively, attributed to the oxidation of PbO to α-PbO_2 (Eq. (8)) [34,40] and of $PbSO_4$ to β-PbO_2 (Eq. (9)). The cathodic peak at 1.05 V/ESC is attributed to the reduction of β-PbO_2 to $PbSO_4$. The results show that the conversion between β-PbO_2 and $PbSO_4$ phases is a reversible process [40].

Based on the obtained results, we tried to find a correlation between lead dioxide particles activity and CV parameters (Fig. 6(c)). Anodic and cathodic current peaks are increased when the cycle number of CV increased. These results could be related to the electroactivity of the materials. Also, the decrease in particle leads to size increase in the active surface which is taking part in the electrode reactions [44].

Oxidation in $AS30/PbO_2$ interface shows a different behavior (reaction) from Pb/PbO_2 anode and a similar one regarding to the substrate and the PbO_2 film which leads to the following conclusion: the stainless steel is an accessible surface with partial passivation after the electrode position of PbO_2 layer because of the current density decrease. The peak intensity reduction on $AS30/PbO_2$ anode would be directly related to the amount of deposited α-PbO_2 and β-PbO_2 forms.

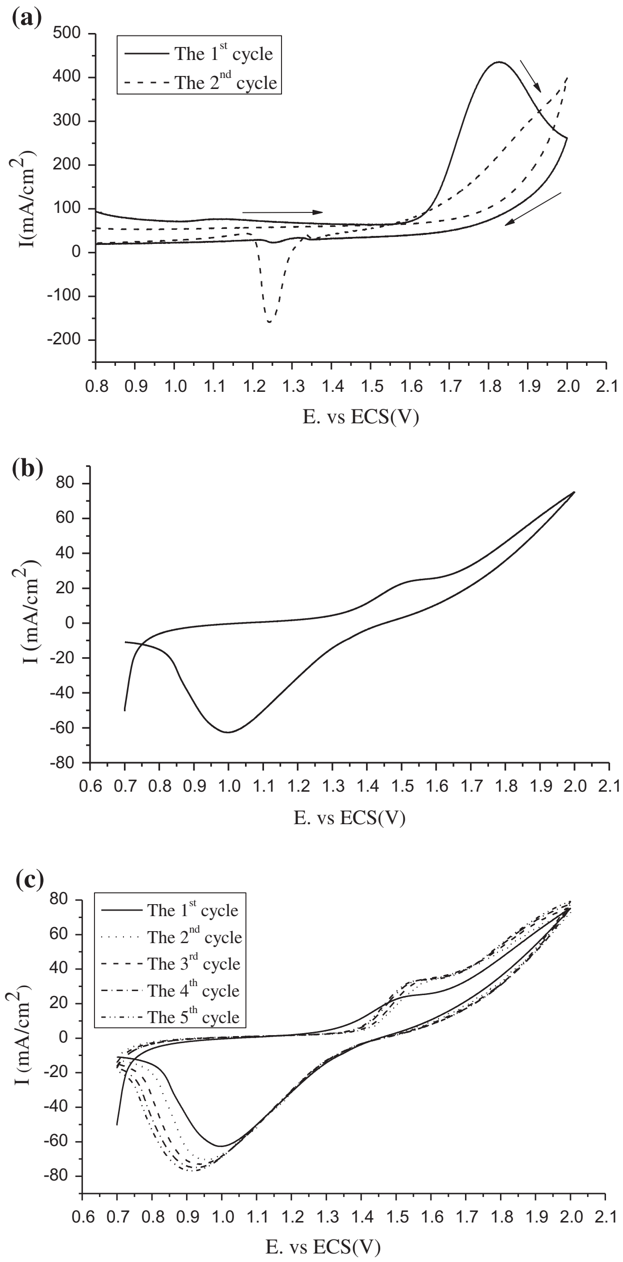

Fig. 6. CV curves for the pure lead (a), Pb/PbO_2 (b) and during five cycles (c) for Pb/PbO_2 in 0.5 M sulfuric acid at the scan rate of 50 mV s^{-1}.

Compared to Pb/PbO_2, the absence of oxidation peak in the case of $AS30/PbO_2$ is related to the oxidation of $PbSO_4$ to β-PbO_2 which confirms the results

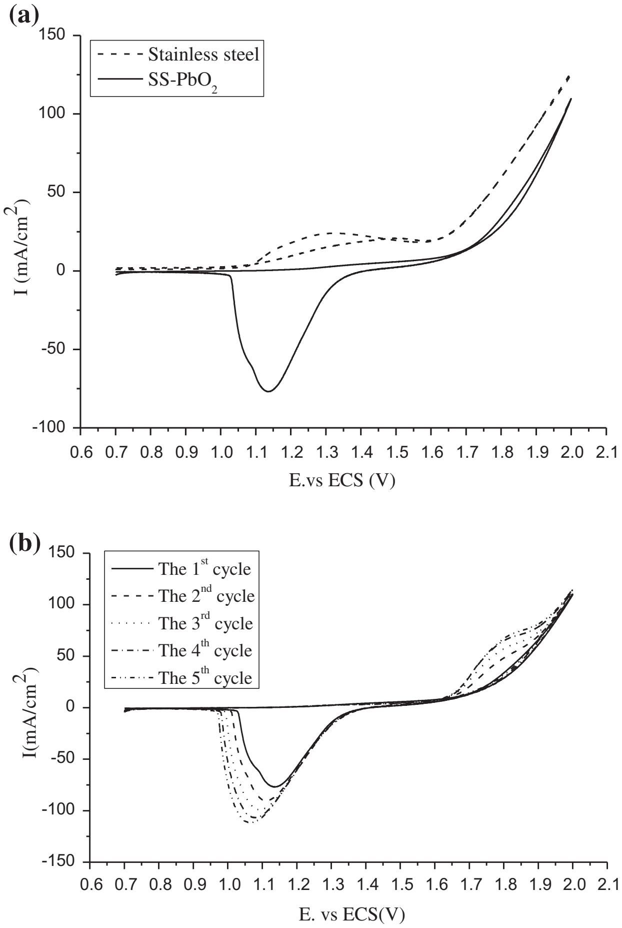

Fig. 7. CV curves of stainless steel and AS30/PbO_2 (a) and (b) the respective five cycles CV curves of AS30/PbO_2 in 0.5 M sulfuric acid at the scan rate of 50 mV s^{-1}.

obtained in the DRX analysis and that shows the absence of $PbSO_4$ layer.

It is clear that in the case of AS30/PbO_2 (Fig. 7(a)), two reduction peaks of lead dioxide to lead sulfate at the potentials of 1.08 V/ESC and 1.16 V/ESC which correspond, respectively, to α and β forms. However, Fig. 7(b) shows that the reduction of this α-modification disappeared completely after the fourth cycle and only β existed and its position shifted slightly to the left. The α structure is more difficult to be reduced to $PbSO_4$ than the β structure due to its compact structure [34]. Conversely, β-PbO_2 is formed due to the oxidation of lead sulfate during the anodic process at 1.8 V/ESC.

3.2.2. *Electrochemical impedance spectroscopy (EIS)*

During further investigation, electrochemical impedance analysis is performed on the basis of two different substrates (Pb and AS30), and two different electrolytes (Na_2SO_4, H_2SO_4). EIS measurements are performed mainly to determine the use of electrodes properties. Pure substrates are also used to understand more the oxide layer/interface. Fig. 8(a)–(d) shows the evolution of the lead impedance whether with or without a PbO_2 film at two pH values. Fig. 9(a)–(d) shows the evolution of the AS30 impedance, according to the same analysis procedure realized on the lead substrate, both with the presence and the absence of the PbO_2 film.

Fig. 10 shows the equivalent electrical circuits used to fit the experimental impedance data of different investigated interfaces. The fitting of Pb with the equivalent circuit of Fig. 10 demonstrates that a first PbO_2 film is deformed with the contact of the atmosphere or electrolyte. A Bode plots are presented in Figs. 8 and 9 showing the dependence of the modulus and the phase vs. frequency. The impedance values roughly indicated by the Bode diagrams are consistent with that obtained by Nyquist patterns (Figs. 8 and 9). Therefore, in the case of lead substrate with and without PbO_2 film, the phases vs. frequency plots show the presence of two times constant behavior which demonstrates the choice of the proposed equivalent circuits used for modeling the EIS measurements. EIS spectra of lead and lead/PbO_2 layer could be represented by a simple equivalent circuit; where the charge-transfer resistance (R_{tc}) and "Constant Phase Element" (CPE_{dl}) reflect the no ideality of the interface. The Warburg impedance (W) is considered due to the main transfers of sulfates and/or H^+ [43]. All the mentioned parameters are in series with the oxide film parameters (CPE_f, R_f). For AS30 with PbO_2 layer, an inductance element (L) is added to the circuit and linked to the partial adhesion between the SS substrate and the PbO_2 film. The obtained impedance spectra (Z modulus vs. frequency) determined that the presence of two relaxation processes can be checked at the higher and intermediate frequency range. In the case of AS30 substrate without PbO_2, the phase vs. frequency plots of stainless steel substrate (Fig. 9(a′) and (c′)) shows a marked difference in the impedance characteristics compared to stainless steel with PbO_2 layer. A loop is detected in the case of stainless steel without PbO_2 film.

The equivalent circuits that are used for modeling the EIS results are shown in Fig. 10 and the theoretical parameters, expressed according to the model for different interfaces, are presented in Tables 1 and 2.

For lead electrode, and according to the comparison of the oxide film parameters (R_f, CPE_f), it appears that the oxide film probably formed at acidic is different from the one at neutral medium with related R_f

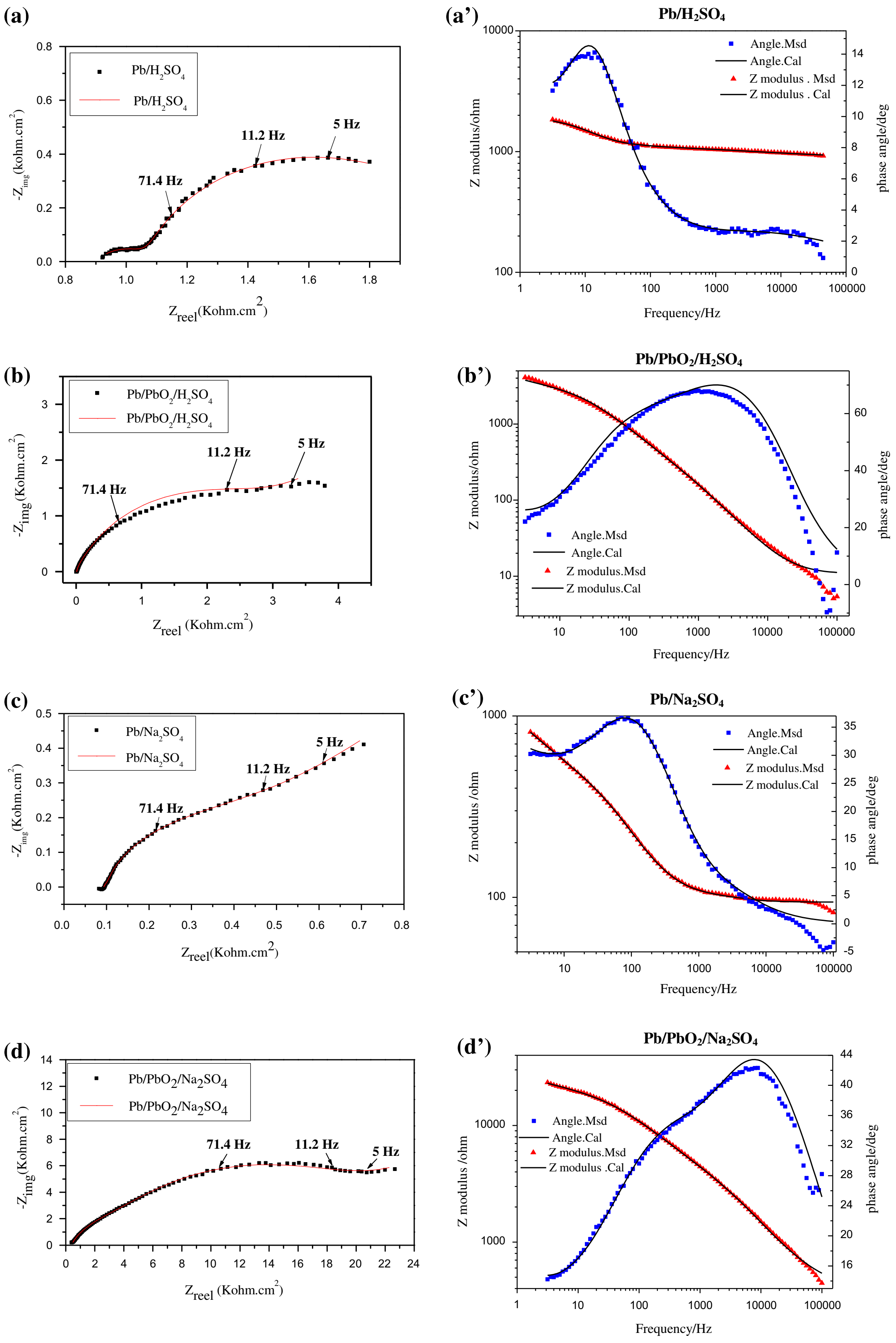

Fig. 8. Nyquist plots for lead substrate with and without PbO_2 film: (a) Pb/H_2SO_4, (b) $Pb/PbO_2/H_2SO_4$, (c) Pb/Na_2SO_4, and (d) $Pb/PbO_2/H_2SO_4$, (■) experimental data (—) solid lines fitted data. (a′), (b′), (c′), and (d′) Bode plots (absolute impedance modulus and phase angle vs. frequency) of different interfaces studied are measured in H_2SO_4 (0.5 M) Na_2SO_4 (0.1 M) as a supporting electrolyte at 25°C, surface area; 2.25 cm^2.

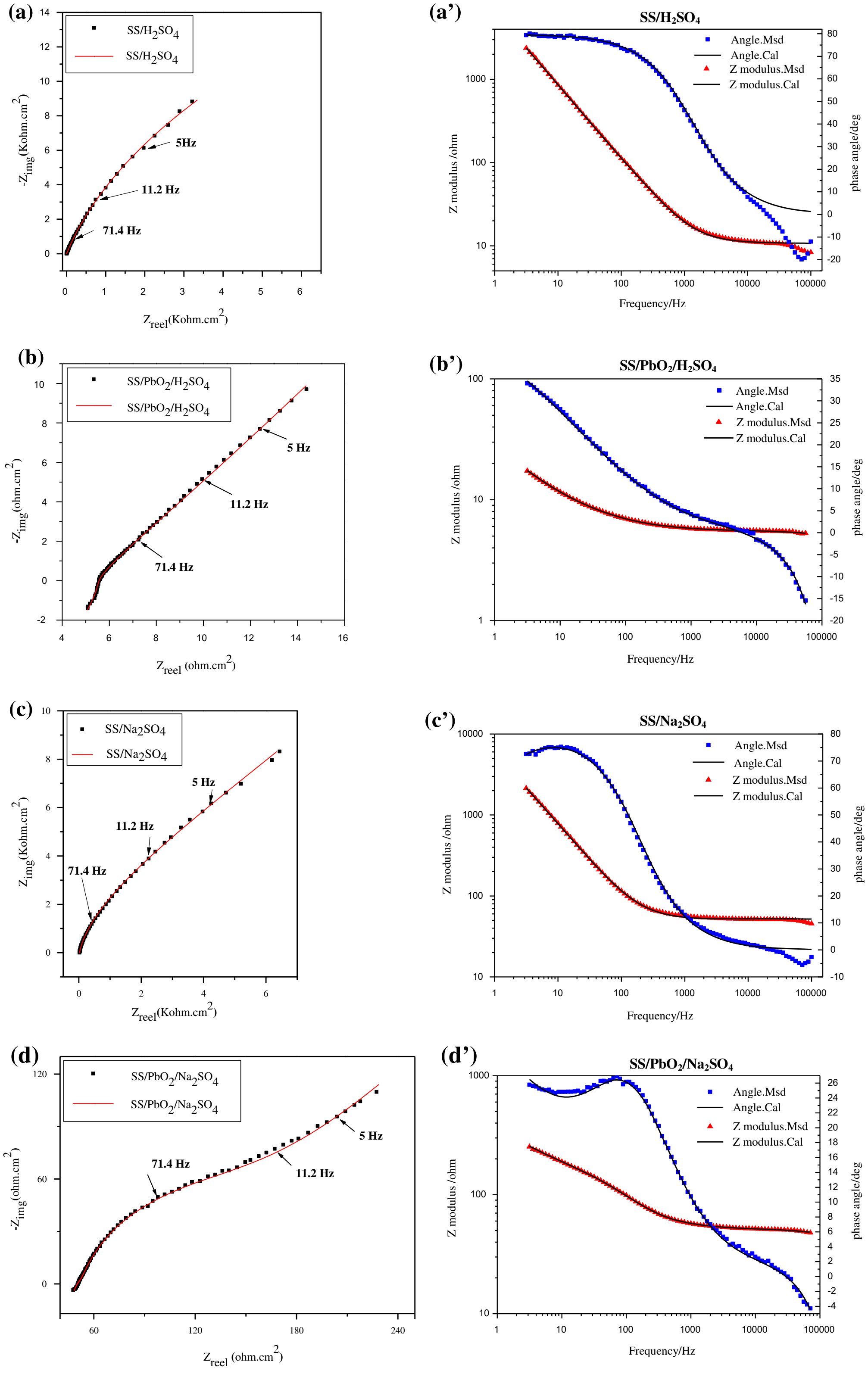

Fig. 9. Nyquist plots for stainless steel substrate (SS) with and without PbO$_2$ film: (a) SS/H$_2$SO$_4$, (b) SS/PbO$_2$/H$_2$SO$_4$, (c) SS/Na$_2$SO$_4$, and (d) SS/PbO$_2$/H$_2$SO$_4$, (■) experimental data (—) solid lines fitted data. (a´), (b´), (c´), and (d´) Bode plots (absolute impedance modulus and phase angle vs. frequency) of different interfaces studied measured in H$_2$SO$_4$ (0.5 M) Na$_2$SO$_4$ (0.1 M) as a supporting electrolyte at 25℃ surface area; 2.25 cm^2.

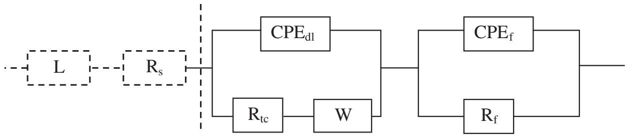

Fig. 10. Equivalent circuits used for the EIS results modeling.

100 times lower. As a conclusion, (i) the formed oxide layer is strongly dependent on the electrolyte and built during stabilization period (ii) the formed oxide is less resistant or more porous when formed at neutral pH. As (CPE_{dl}/R_{tc}) have the same magnitude in the two pH, we can conclude that the presence of the oxide film does not impact on the Pb/electrolyte electron transfer. In acidic solutions for Pb/H_2SO_4 interface, the passivation layer of $PbSO_4$ is formed on Pb. According to Yao et al. [45], the consequence of this lead sulfate layer is to block off the active surface, and, thus to obscure the reaction. The effect of this is later seen on the CPE_{dl} which is reduced comparing to the value detected in neutral medium (Table 1).

As depicted in Table 1, it turned out that the value of the R_{tc} is higher in the case of lead in H_2SO_4 than natural solution, indicating that the lead sulfate layer is more compact and the access of electrolyte ions to the internal layer is stopped [46]. Also, in the case of acidic pH characterized by high R_f; the electrolyte penetrates into the pores of oxide layer [40,47]. This film is not continuous and the covered surface is low to impact strongly on lead interface parameters.

For Pb/PbO_2 electrode, the PbO_2 layer is formed before EIS following Section 2.3.1. The comparison between Pb/electrolyte and Pb/PbO_2/H_2SO_4 demonstrates that the obtained values are similar in magnitude also for (CPE_f/R_f). We can conclude that when both are performed in acidic pH, the pH is an important parameter influencing the oxide film proprieties. This conclusion is corroborated by the results obtained in neutral pH of Pb/PbO_2 interface as values of (CPE_f/R_f) are totally different. However, it can be noted that the PbO_2 film exhibits higher resistance in Na_2SO_4 electrolyte than H_2SO_4 one.

Meanwhile, in the present case, inside the porous structure, diffusion is limited by the pore geometry and has decreased in the CPE_{dl}, we can sum up that the electrode with PbO_2 layer in H_2SO_4 solution becomes blocked with $PbSO_4$. Chun Nan Ho et al. [48] demonstrates that the decrease of the CPE_{dl} values is attributed also to a progressive exclusion of the porous structure due to small bubbles clogging the pores. Additionally, the presence of the nonconductive forms ($PbSO_4$ and tet-PbO) in PbO_2 film deposit on lead substrate (found by DRX analysis) can also contribute to the reduction of CPE_{dl} value which depends on the gradients in dielectric properties (composition/phase) of the coating [45,49,50].

As expected, similar behavior is obtained in the Fig. 9(a) and (c). The high value of R_{tc} is linked to the passivation layer of stainless steel [51,52]. The AS30/PbO_2 modifies completely the interface with a strong decrease of R_{tc} to be similar to Pb/PbO_2 interface: Fig. 9(b) and (d). However, the oxide film resistance

Table 1
EIS fitting parameters of lead without and with PbO_2 layer (influence of pH)

		CPE_{dl} (S $cm^{-2}s^n$) ($\times 10^{-6}$)	N	R_{tc} (Ω cm^2)	W (S $cm^{-2}s^{1/2}$) ($\times 10^{-4}$)	CPE_f (S $cm^{-2}s^n$) ($\times 10^{-6}$)	n	R_f (Ω cm^2)	χ^2
In H_2SO_4	Pb	13.09	0.49	465.2	2.54	14.4	1	9.99 10^2	6.37×10^{-5}
(pH 0.52)	Pb/PbO_2	1.65	1	108	1.21	6.09	0.87	2.21 10^3	2.80×10^{-2}
In Na_2SO_4	Pb	19.2	0.86	367.5	4.18	7.09	1	5.09	1.11×10^{-3}
(pH 6.8)	Pb/PbO_2	0.28	0.76	2,351	42.17	1.37	0.64	1.76 10^4	1.59×10^{-3}

Table 2
EIS fitting parameters of AS30 without and with PbO_2 layer (influence of pH)

		L (10^{-6})	CPE_{dl} (S $cm^{-2}s^n$) ($\times 10^{-5}$)	N	R_{tc} (Ω cm^2)	W (S $cm^{-2}s^{1/2}$) ($\times 10^{-4}$)	CPE_f (S $cm^{-2}s^n$) ($\times 10^{-6}$)	n	R_f (Ω cm^2)
In H_2SO_4	AS30	–	15.03	0.88	5.10 10^4	8.59	–	–	–
(pH 0.52)	AS30/PbO_2	8.38	800.4	0.62	12.26	75.91	0.16	0.99	5.47
In Na_2SO_4	AS30	–	6.62	0.90	4.90 10^3	1.01	–	–	–
(pH 6.8)	AS30/PbO_2	19.7	7.08	0.81	111.3	15.27	1.01	0.59	52.41

R_f on AS30 is at least 100 less than Pb indicating that the reaction surface of the PbO_2 film on Pb is 100 times more resistive than that of the film on AS30 substrate; suggesting that the PbO_2 layer is totally different in proprieties, more porous or adherent. The presence of inductance in the equivalent circuit confirms the latter interpretation.

3.3. Degradation test on PbO_2 anodes: bulk electrolysis

The objective of this work is to investigate the performance of the PbO_2 film electrodeposited on lead as a reference, and on the stainless steel for the AO of an azo dye, as a pollutant model.

The organic degradation of the pollutant on PbO_2 is proved to be a free-radical mechanism as follow [53]:

$$PbO_2 + H_2O_{ads} \rightarrow PbO_2(^{\bullet}OH)_{ads} + H^+ \qquad (11)$$

It was reported that lead dioxide electrode is a hydrated one, and the electrogenerated hydroxyl radicals are expected to be more strongly adsorbed on its surface. This behavior makes lead dioxide anode very reactive toward organic oxidation. The degradation reaction of the organic pollutants with adsorbed hydroxyl radicals is completed by forming carbon dioxide and water.

In order to compare the performance of the prepared electrodes on the treatment capacity by applying the same current density (equal to 25 mA/cm^2), and using the same cathode (stainless steel), the AO using electrodes Pb/PbO_2 and $AS30/PbO_2$ as anodes are used for the degradation (as described in Section 2.6).

The results obtained for the color and COD removals are presented by Figs. 11 and 12. The highest percentage of color removals is reached in the acidic medium. After 6 h treatment, the color removal by Pb/PbO_2 and $AS30/PbO_2$ anodes achieved 95 and 91%, respectively. A partial detachment of PbO_2 layer is observed after 60 min in the case of AS30.

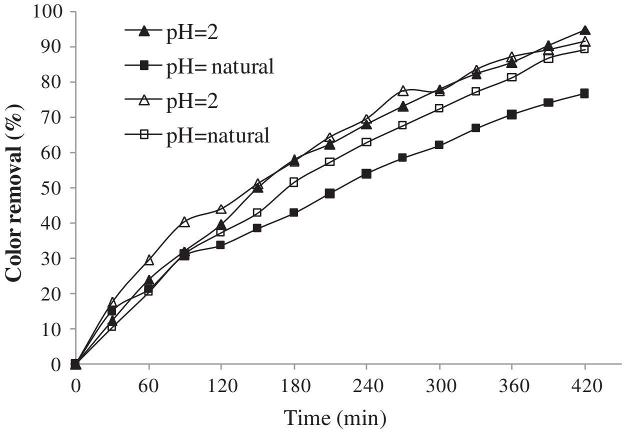

Fig. 11. The color removal during the electrolysis of Amaranth (E120) on the Pb/PbO_2 anode (solid symbols) and $AS30/PbO_2$ anode (Open symbols). Operative conditions: $C_{0Amaranth}$, 0.05 mM; flow rate, 138 l h^{-1}; T, 25°C; applied current density, 25 mA cm^{-2}; pH 2 and natural.

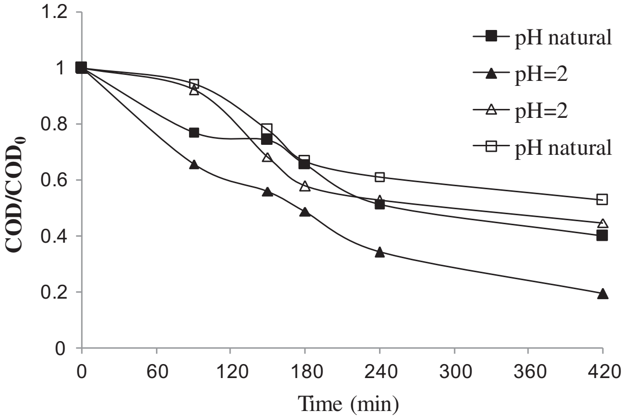

Fig. 12. Evolution of the COD removal during the oxidation on Pb/PbO_2 anode (solid symbols) and $AS30/PbO_2$ anode (Open symbols), Operation conditions: flow-rate: 138 l h^{-1}, 25°C; applied current density, 25 mA cm^{-2}; pH 2 and natural.

The influence of pH is quite more important in the case of the lead electrode. According to Chen et al. [40], the presence of appropriate amount of α-PbO_2 in the mixture of α-and β-PbO_2 may enhance the use of β-PbO_2, the surface area in the case of tetrahedral structure is more important than that of the orthorhombic one. Also, the β-PbO_2 form would be more effective than the α-PbO_2 form because of the oxygen over potential evolution of β-PbO_2 that is higher than that of α-PbO_2 [53]. The conductivity of the β-phase tends to be an order of magnitude higher than that of the α-phase, due to the higher electron mobility. Advanced electrochemical water treatments preferably require the β-phase because its porous structure provides a larger active surface area for anodic applications; therefore, the increase in the active surface area will elevate the formation of OH· radicals and will favorite the degradation of organic compounds [54]. However, the co-existence of α- and β-PbO_2 phases is very necessary to improve the electrochemical performance of the positive electrode [38], and both of these forms in anodic layer depend strongly, not only on the preparation conditions (pH-medium and temperature), but also on the technical preparation [55]. Thus, and as expected, the electrolysis properties of Pb/PbO_2 electrode are more efficient than the $AS30/PbO_2$ electrode and that could have been better if its life service is longer (low adherence persistence).

It is generally considered that the initial pH of electrolyte plays a significant role in the electrochemical degradation of azo dye and the COD removals in Pb/PbO_2 and $AS30/PbO_2$ anodes [9,56,57].

In order to study the influence of pH on the electrolysis (Fig. 12), the comparison of the COD/COD_0 trend under two different pHs, during the oxidation with Pb/PbO_2 and $AS30/PbO_2$ anodes is performed. In acidic conditions, the COD removal is higher than that in natural ones, and the oxygen evolution potential is relatively high, which leads to a better degradation efficiency than in neutral conditions. The Pb/PbO_2 anode reached about 82% COD removal against 76% for $AS30/PbO_2$ anode.

In this work, $AS30/PbO_2$ anode leads to a lower degradation of the dye than the Pb/PbO_2 anode used as a reference for comparison. This result is due to the detected low adherence persistence, and it is in agreement with the EIS results, as in an acidic medium, the CPE_{dl} is higher and the R_f is lower for $AS30/PbO_2$ anode.

Table 3 presents the first-order constant rate (k_{app}) and the R^2 values of the discoloration and COD removal obtained for both electrodes Pb/PbO_2 and $AS30/PbO_2$ anodes at pH 2 and natural:

At pH 2, Amarath solution has a higher oxidation rate than when the pH is natural especially for the Pb/PbO_2 anode. As shown in Table 3, the K_{app} COD value at pH 2 is about 1.7 times higher than that of a natural pH for the Pb/PbO_2 anode, and almost the same with the $AS30/PbO_2$ anode, while the $K_{app\ dis}$ increased 1.5 times in the acidic pH when compared by natural pH for Pb/PbO_2.

The better performance presented by the PbO_2 electrode in the degradation of the Amaranth E123 dye is studied according to the energy consumption, and for large-scale application. Besides, the energy consumption has a high impact on the treatment costs.

Table 3
Amaranth degradation kinetics by Pb/PbO_2 and $AS30/PbO_2$ anodes

	Pb/PbO_2		$AS30/PbO_2$	
pH	2	Natural	2	Natural
k_{app} dis (10^{-3} min^{-1})	5.2	3.4	5.4	4.7
R^2	0.98	0.99	0.98	0.95
k_{app}COD (10^{-3} min^{-1})	4	2.3	2.2	1.7
R^2	0.99	0.96	0.87	0.9
$E_c{}^a$(kWh g DCO^{-1})	0.23	0.41	0.39	0.50
CE*(%)	10.53	6.70	6.70	5.42

[a] Quantity estimated at 420 min.

The effect of pH on E_c and CE is presented in Table 3. After 6 h of treatment, the CE kept a relatively high value, 10.53% at pH 2, for the Pb/PbO_2 anode in comparison to $AS30/PbO_2$ (6.70%). The Pb/PbO_2 anode consumes less energy than $AS30/PbO_2$ anode. For example, at pH 2, 0.23 and 0.39 kWh g COD^{-1} are consumed for Pb/PbO_2 and $AS30/PbO_2$ anodes, respectively. Energy consumption is higher at natural pH than at an acid one.

These results show the high performance of PbO_2 oxidation when treating textile wastewaters. However, this electrochemical process AO could be a feasible treatment method when it is compared to other wastewater treatments (e.g. UV irradiation, Fenton, adsorption) reducing significantly the cost and treatment time [58].

4. Conclusion

In this work, two electrodes (Pb/PbO_2 and $AS30/PbO_2$) were prepared by electrodeposition (pulsed and galvanostatically) and used as anodes for degradation of Amarath (E123) at two pH (natural and acidic). The results of SEM, AFM, and XRD showed that the crystal size and the nature of the mixtures microparticles PbO_2. It is proved that the β-PbO_2 is dominant in two cases, but in the case of stainless steel substrate; $PbSO_4$ and tet-PbO forms do not exist. The electrochemical behavior of studied anodes using CV and EIS techniques has demonstrated that the different interfaces studied depend on the nature of the substrate. The absence of oxidation peak related to oxidation of $PbSO_4$ to β-PbO_2 and after five cycles, the reduction of α form is disappeared and only the β existed. And as shown, the EIS analysis is the higher values of R_f and CPE_{dl} into stainless steel and PbO_2 film. This result is related to a better adherence between film and substrate. It is expected because the thickness and the cristallinity of oxide layer are more relevant in electrodeposited galvanostatically on pure lead.

After degradation test, 95 and 91% of color removal, 82 and 76% of COD removals were achieved using Pb/PbO_2 and $AS30/PbO_2$ anodes, respectively. This is due to a higher production of hydroxyl radicals in acidic pH on the electrode surface during electrolysis that lead to remarkably higher current efficiency and lower specific energy consumption. Moreover, even when using the $AS30/PbO_2$ anode, a problem of detachment of film is observed; however, good removal efficiency was obtained.

Acknowledgment

This research is carried out with the support of International Foundation for Science (IFS), Sweden, by a research following ship to CP: Hanene Akrout–Baccour.

References

[1] G. Chen, Electrochemical technologies in wastewater treatment, Sep. Purif. Technol. 38 (2004) 11–41.

[2] O. Scialdone, A. Galia, L. Gurreri, S. Randazzo, Electrochemical abatement of chloroethanes in water: Reduction, oxidation and combined processes, Electrochim. Acta 55 (2010) 701–708.

[3] A. Atyaoui, L. Bousselmi, H. Cachet, P. Pu, E.M.M. Sutter, Influence of geometric and electronic characteristics of TiO_2 electrodes with nanotubular array on their photocatalytic efficiencies, J. Photochem. Photobiol., A 224 (2011) 71–79.

[4] M. Panizza, G. Cerisola, Applicability of electrochemical methods to carwash wastewaters for reuse. Part 1: Anodic oxidation with diamond and lead dioxide anodes, J. Electroanal. Chem. 638 (2010) 28–32.

[5] L. Mansouri, H. Mohammed, C. Tizaoui, L. Bousselmi, Heterogeneous catalytic ozonation of diethyl phthalate, J. Desalin. Water 51 (2013) 6698–6710.

[6] M. Panizza, C.A. Martinez-Huitle, Role of electrode materials for the anodic oxidation of a real landfill leachate—Comparison between Ti–Ru–Sn ternary oxide, PbO_2 and boron-doped diamond anode, Chemosphere 90 (2013) 1455–1460.

[7] F. Zaviska, P. Drogui, J.-F. Blais, G. Mercier, Electrochemical treatment of bisphenol-A using response surface methodology, J. Appl. Electrochem. 42 (2012) 95–109.

[8] N.B. Taher, A. Savall, Electrochemical removal of phenol in alkaline solution: Contribution of the anodic polymerization on different electrode materials, Electrochim. Acta 54 (2009) 4809–4816.

[9] H.S. Awad, N.A. Ghalwa, Electrochemical degradation of Acid Blue and Basic Brown dyes on Pb/PbO_2 electrode in the presence of different conductive electrolyte and effect of various operating factors, Chemosphere 61 (2005) 1327–1335.

[10] C. Comninellis, C. Pulgarin, Anodic oxidation of phenol for waste water treatment, J. Appl. Electrochem. 21 (1991) 703–708.

[11] J.L. Nava, M.A. Quiroz, C.A. Martinez-Huitle, Electrochemical treatment of synthetic wastewaters containing Alphazurine A dye: Role of electrode material in the color and COD removal, J. Mex. Chem. Soc. 52 (2008) 249–255.

[12] J.Y. Choi, Y.-J. Lee, J. Shin, J.-W. Yang, Anodic oxidation of 1,4-dioxane on boron-doped diamond electrodes for wastewater treatment, J. Hazard. Mater. 179 (2010) 762–768.

[13] N. Abdessamad, H. Akrout, G. Hamdaoui, K. Elghniji, M. Ksibi, L. Bousselmi, Evaluation of the efficiency of monopolar and bipolar BDD electrodes for electrochemical oxidation of anthraquinone textile synthetic effluent for reuse, Chemosphere 93 (2013) 1309–1316.

[14] F.L. Migliorini, N.A. Braga, S.A. Alves, M.R.V. Lanza, M.R. Baldan, N.G. Ferreira, Anodic oxidation of wastewater containing the Reactive Orange 16 Dye using heavily boron-doped diamond electrodes, J. Hazard. Mater. 192 (2011) 1683–1689.

[15] C.A. Martínez-Huitle, E.V. dos Santos, D.M. de Araújo, M. Panizza, Applicability of diamond electrode/anode to the electrochemical treatment of a real textile effluent, J. Electroanal. Chem. 674 (2012) 103–107.

[16] C. Yuan, Y.-D. Dai, C.-H. Hung, Regeneration of spent carbon nanotube by electrokinetic process with binary metallic oxide electrodes of $MnO_2/TiRuO_2/Ti$, and PbO_2/Ti, Sep. Purif. Technol. 79 (2011) 238–245.

[17] D. Devilliers, T. Baudin, M.T. Dinh Thi, E. Mahé, Selective electrodeposition of PbO_2 on anodised-polycrystalline titanium, Electrochim. Acta 49 (2004) 2369–2377.

[18] Y. Song, G. Wei, R. Xiong, Structure and properties of PbO_2–CeO_2 anodes on stainless steel, Electrochim. Acta 52 (2007) 7022–7027.

[19] V. Sáez, M.D. Esclapez, A.J. Frías-Ferrer, P. Bonete, I. Tudela, M.I. Díez-García, J. González-García, Lead dioxide film sonoelectrodeposition in acidic media: Preparation and performance of stable practical anodes, Ultrason. Sonochem. 18 (2011) 873–880.

[20] H. Li, Y. Chen, Y. Zhang, W. Han, X. Sun, J. Li, L. Wang, Preparation of Ti/PbO_2–Sn anodes for electrochemical degradation of phenol, J. Electroanal. Chem. 689 (2013) 193–200.

[21] D. Zhou, L. Gao, Effect of electrochemical preparation methods and properties of PbO_2 anodic layer, Electrochim. Acta 53 (2007) 2060–2064.

[22] V. Suryanarayanan, I. Nakazawa, S. Yoshihara, T. Shirakashi, The influence of electrolyte media on the deposition/dissolution of lead dioxide on boron-doped diamond electrode—A surface morphologic study, J. Electroanal. Chem. 592 (2006) 175–182.

[23] A. Mukimin, K. Wijaya, A. Kuncaka, Oxidation of remazol brilliant blue r (RB.19) with *in situ* electrogenerated active chlorine using Ti/PbO_2 electrode, Sep. Purif. Technol. 95 (2012) 1–9.

[24] S. Abaci, U. Tamer, K. Pekmez, A. Yildiz, Performance of different crystal structures of PbO_2 on electrochemical degradation of phenol in aqueous solution, Appl. Surf. Sci. 240 (2005) 112–119.

[25] X. Hao, L. Jingjing, Y. Wei, W. Chu, Preparation and characterization of titanium based PbO_2 electrodes doped with some common elements, J. Rare Metal. Mat. Eng. 42 (2013) 885–890.

[26] L.S. Andrade, L.A.M. Ruotolo, R.C. Rocha-Filho, N. Bocchi, S.R. Biaggio, J. Iniesta, V. García-Garcia, V. Montiel, On the performance of Fe and Fe,F doped Ti–Pt/PbO_2 electrodes in the electrooxidation of the Blue Reactive 19 dye in simulated textile wastewater, Chemosphere 66 (2007) 2035–2043.

[27] K. Pan, M. Tian, Z.-H. Jiang, B. Kjartanson, A. Chen, Electrochemical oxidation of lignin at lead dioxide nanoparticles photoelectrodeposited on TiO_2 nanotubearrays, Electrochim. Acta 60 (2012) 147–153.

[28] Y. Zheng, W. Su, S. Chen, X. Wu, X. Chen, Ti/SnO_2–Sb_2O_5-RuO_2/α-PbO_2/β-PbO_2 electrodes for pollutants degradation, J. Chem. Eng. 174 (2011) 304–309.

[29] W. Han, Y. Chen, L. Wang, X. Sun, J. Li, Mechanism and kinetics of electrochemical degradation of isothiazolin-ones using Ti/SnO_2–Sb/PbO_2 anode, Desalination 276 (2011) 82–88.

[30] C.A. Martínez-Huitle, M.A. Quiroz, C. Comninellis, S. Ferro, A. Battisti, Electrochemicals incineration of chloranilic acid using TI/Iro_2, Pb/PbO_2 and BDD electrodes, Electrochim. Acta 50 (2004) 949–956.

[31] Y. Yao, M. Zhao, C. Zhao, H. Zhang, Preparation and properties of PbO_2-ZrO_2 nanocomposite electrodes by pulse electrodeposition, Electrochim. Acta 117 (2014) 453–459.

[32] M.M. Burashnikova, I.A. Kazarinov, I.V. Zotova, Nature of contact corrosion layers on lead alloys: A study by impedance spectroscopy, J. Power Sources 207 (2012) 19–29.

[33] F. Mohammadi, T. Nickchi, M.M. Attar, A. Alfantazi, EIS study of potentiostatically formed passive film on 304 stainless steel, Electrochim. Acta 56 (2011) 8727–8733.

[34] I. Yahiaoui, F. Aissani-Benissad, F. Fourcade, A. Amrane, Removal of tetracycline hydrochloride from water based on direct anodic oxidation (Pb/PbO_2 electrode) coupled to activated sludge culture, J. Chem. Eng. 221 (2013) 418–425.

[35] H. An, H. Cui, W. Zhang, J. Zhai, Y. Qian, X. Xie, Q. Li, Fabrication and electrochemical treatment application of a microstructured TiO_2-NTs/Sb–SnO_2/PbO_2 anode in the degradation of C.I. Reactive Blue 194 (RB 194), J. Chem. Eng. 209 (2012) 86–93.

[36] S.C. Elaoud, M. Panizza, G. Cerisola, T. Mhiri, Electrochemical degradation of sinapinic acid on a BDD anode, Desalination 272 (2011) 148–153.

[37] M. Hamza, R. Abdelhedi, E. Brillas, I. Sirés, Comparative electrochemical degradation of the triphenylmethane dye Methyl Violet with boron-doped diamond and Pt anodes, J. Electroanal. Chem. 627 (2009) 41–50.

[38] L. Zerroual, R. Fitas, B. Djellouli, N. Chelali, Relationship between water departure and capacity loss of α and β-PbO_2 using an all solid-state system: Estimation of proton diffusion coefficient, J. Power Sources 158 (2006) 837–840.

[39] T. Chen, H. Huang, H. Ma, D. Kong, Effects of surface morphology of nanostructured PbO_2 thin films on their electrochemical properties, Electrochim. Acta 88 (2013) 79–85.

[40] D. Devilliers, M.T.D. Thi, E. Mahé, V. Dauriac, N. Lequeux, Electroanalytical investigations on electrodeposited lead dioxide, J. Electroanal. Chem. 573 (2004) 227–239.

[41] V. Suryanarayanan, I. Nakazawa, S. Yoshihara, T. Shirakashi, The influence of electrolyte media on the deposition/dissolution of lead dioxide on boron-doped diamond electrode—A surface morphologic study, J. Electroanal. Chem. 592 (2006) 175–182.

[42] D. Pavlov, A. Kirchev, M. Stoycheva, B. Monahov, Influence of H2SO4 concentration on the mechanism of the processes and on the electrochemical activity of the Pb/PbO_2/$PbSO_4$ electrode, J. Power Sources 137 (2004) 288–308.

[43] C. Yang, Y. Ko, S.-M. Park, Fourier transform electrochemical impedance spectroscopic studies on anodic reaction of lead, Electrochim. Acta 78 (2012) 615–622.

[44] H. Karami, B. Kafi, S.N. Mortazavi, Effect of particle size on the cyclic voltammetry parameters of nanostructured lead dioxide, Int. J. Electrochem. Sci. 4 (2009) 414–424.

[45] Z. Yao, Z. Jiang, F. Wang, Study on corrosion resistance and roughness of micro-plasma oxidation ceramic coatings on Ti alloy by EIS technique, Electrochim. Acta 52 (2007) 4539–4546.

[46] Z.-G. Ye, H.-M. Meng, D.-B. Sun, Electrochemical impedance spectroscopic (EIS) investigation of the oxygen evolution reaction mechanism of Ti/$IrO_2 + MnO_2$ electrodes in 0.5m H_2SO_4 solution, J. Electroanal. Chem. 621 (2008) 49–54.

[47] Y. Li, L.X. Jiang, X.J. Lv, Y.Q. Lai, H.L. Zhang, J. Li, Y.X. Liu, Oxygen evolution and corrosion behaviors of co-deposited Pb/Pb-MnO_2 composite anode for electrowinning of nonferrous metals, Hydrometallurgy 109 (2011) 252–257.

[48] ChN Ho, B.J. Hwang, Effect of hydrophobicity on the hydrophobic modified polytetrafluoroethylene/PbO_2, electrode towards oxygen evolution, J. Electroanal. Chem. 377 (1994) 177–190.

[49] J.A. Bialacki, N.A. Hampson, The a.c. impedance of porous PbO_2 on a lead support in sulphuric acid, Surf. Technol. 23 (1984) 117–125.

[50] D.G. Li, D.R. Chen, J.D. Wang, H.S. Chen, Influences of temperature, H_2SO_4 concentration and Sn content on corrosion behaviors of Pb/Sn alloy in sulfuric acid solution, J. Power Sources 196 (2011) 8789–8801.

[51] L. Ćurković, H.O. Ćurković, S. Salopek, M.M. Renjo, S. Šegota, Enhancement of corrosion protection of AISI 304 stainless steel by nanostructured sol–gel TiO_2 films, Corros. Sci. 77 (2013) 176–184.

[52] N. Diomidis, J.-P. Celis, P. Ponthiaux, F. Wenger, Tribocorrosion of stainless steel in sulfuric acid: Identification of corrosion–wear components and effect of contact area, Wear 269 (2010) 93–103.

[53] N.A. Ghalwa, H.M. Abu-Shawish, H.M. Tamous, H. Al Harazeen, Determination of electrochemical degradation of E102 dye at lead dioxide-doped carbon electrodes using some potentiometric and spectrophotometric methods, J. Chim. 3 (2013) 1–6.

[54] I. Sirés, C.T.J. Low, C. Ponce-de-León, F.C. Walsh, The characterization of PbO_2-coated electrodes prepared from aqueous methanesulfonic acid under controlled deposition conditions, Electrochim. Acta 55 (2010) 2163–2172.

[55] I.-H. Yeo, S. Wen, S. Mho, Effect of interfacial oxides on the electrochemical activity of lead dioxide film electrodes on a Ti substrate, Anal. Sci. 26 (2010) 39–44.

[56] Y. Samet, S.C. Elaoud, S. Ammar, R. Abdelhedi, Electrochemical degradation of 4-chloroguaiacol for wastewater treatment using PbO_2 anodes, J. Hazard. Mater. 138 (2006) 614–619.

[57] H. Lin, J. Niu, J. Xu, Y. Li, Y. Pan, Electrochemical mineralization of sulfamethoxazole by Ti/SnO_2-Sb/Ce-PbO anode: Kinetics, reaction pathways, and energy cost evolution, Electrochim. Acta 97 (2013) 167–174.

[58] J.H.B. Rocha, M.M.S. Gomes, N.S. Fernandes, D.R. da Silva, C.A. Martínez-Huitle, Application of electrochemical oxidation as alternative treatment of produced water generated by Brazilian petrochemical industry, Fuel Process. Technol. 96 (2012) 80–87.